GeoScienceWorld
Lithosphere
Volume 2022, Article ID 4328618, 18 pages
https://doi.org/10.2113/2022/4328618

Lithosphere

Research Article

Research on Roof Structure and Determination of Working Resistance of Shallow Buried Single Key Stratum Based on Grid Drillhole Field Method

Yanpeng He[1,2] **and Qingxiang Huang**[1,2]

[1]*School of Energy Engineering, Xi'an University of Science and Technology, Shaanxi, Xi'an 710054, China*
[2]*Key Laboratory of Western Mine Exploitation and Hazard Prevention with Ministry of Education, Xi'an University of Science and Technology, Xi'an, Shaanxi 710054, China*

Correspondence should be addressed to Qingxiang Huang; huangqx@xust.sn.cn

Received 1 December 2021; Accepted 23 February 2022; Published 28 March 2022

Academic Editor: Yonghui Wu

The roof structure of the stope is the core of revealing the weighting mechanism and determining the working resistance of support. The Shenfu Dongsheng coal field of China has abundant reserves of shallow coal seam. The phenomena of strong ground pressure and step subsidence caused by the mining of shallow buried single key stratum (SBSKS) poses a serious threat to the fragile environment. Revealing the shape and movement process of roof structure of SBSKS is the primary prerequisite for ensuring safe mining of working face. Firstly, the field measurement technology of the space grid-like drill field was developed to construct vertical holes and incline holes in the auxiliary headgate gateway and tailgate airway ahead of the working face and to obtain the measured data of the broken position and vertical displacement of the roof by the drilling peep and multipoint displacement. Secondly, the key parameters of the stope roof were analyzed by the grid drillhole filed method, for example, the inclined roof break angle, the rotation angle, the thickness of equivalent immediate roof (EIR), and the roof structure-articulated level and shape. Then, we combined with the mining face comparison of compression laws revealing the time and space relationship between the movement of the roof structure and the roof weighting, and three more dangerous states of the roof were determined. Finally, the roof structure of SBSKS is moved upward through the field research on the 22201 working face, the "high step rock beam" structure and the advanced breaking position of the roof are obtained, and the calculation equation of the support resistance in large mining height face is given. The research results provide scientific guidance for the safety of SBSKS coal seam and provide technical support for green mining in ecologically fragile mining areas.

1. Introduction

In the process of underground coal mining, controlling overburden movement is the primary issue. Only by grasping the possible formation structure and its activity law after the rock mass is destroyed can the relationship of "support-surrounding rock" be reasonably used, controlling the safety of the stope economically and ensuring the safety of personnel and equipment [1–4]. The overburden structure is not an artificial structure. Expecting to obtain the morphological characteristics of overburden failure, filed observation drillhole, and peeking [2, 5], advanced testing methods are employed at the filed research, such as electromagnetic seismic [6, 7], microseismic [8–10], and optical fibers [11]. In the laboratory, physical simulation [12–16] and numerical simulation [17–19] are applied to simulate the overlying strata movements. The roof structure is analyzed and deduced through the acquisition, analysis, and processing of characteristic data. The commonly used test methods for field measurement of surrounding rock deformation are shown in Table 1.

Roof weighting is the performance of roof structure movement. Mastering the movement law of the roof structure and establishing the mechanical model of the roof structure are important bases to reveal the mechanism of weighting and determine reasonable support resistance.

Table 1: The commonly used test methods for field measurement of surrounding rock deformation.

Test method	Method principle	Conditions	Application
Drilling rinse liquid measurement	The fracture development and permeability change of rock mass are evaluated by recording the change of injected rinse liquid or water injection amount.	The original geology conditions are few cracks, faults, etc.	Drilling construction positions are usually placed on the ground, which can obtain the structural forms of deformation and failure of roof formation through testing.
Drilling water injection observation			Usually layout drilling construction position in the underground roadway and water injection can obtain the surrounding rock crack.
Drilling TV observation	The development of the fissures in the borehole can be visually observed through the image.	The surrounding rock conditions of the borehole are better.	It can be implemented both on the ground and underground. Underground drilling TV method is usually used to achieve direct observation of rock destroyed.
Microseismic monitoring	When the rock mass ruptures, it generates weak seismic wave energy, which can be judged by obtaining the number of microseismic events and energy.	Applicability is not affected by environmental and geological conditions.	Mainly through the observation system arranged underground in the coal body, in order to obtain the failure characteristics of the surrounding rock.
Seismic prospecting technique	When the rock is destroyed, the elastic parameters of the formation rock change. Analyze by acquiring seismic wave parameters.	Not limited by the construction environment.	Ground-based source excitation and observation system can obtain the development characteristics of rock mass fissures of mining space in roof and floor within a certain depth.
Optical fiber testing technology	During the movement of rock, the physical properties of the original rock are changed, resulting in compression or stretching of the fracture.	Not limited by the construction environment. It is suitable for long-term and dynamic monitoring.	Observation system can be arranged on the ground and underground, and the ground system mainly observes the roof, while the full-space observation of roof and two sides in the underground can be realized.
Bolt displacement monitoring	When the overburden is broken in mining, we can observe the displacement of the roof, floor, roadway section, and bolt, etc.	It is usually observed in the underground, and the surrounding rock is more stable.	The test instruments are arranged in the surrounding rock of the roadway, and the displacement of the roof and floor of surrounding rocks can be obtained
Hydraulic support resistance		Not limited.	By obtaining the roof pressure of the hydraulic support column of the working face or roadway.
Other roadway section measurement		It is not limited by test conditions, but the results are affected by the test instruments.	The test instruments are in the cross-section of the roadway to measure the displacement of the roof, floor, and the two sides.

The "voussoir beam" theory and the key stratum theory in stope ground control are proposed, which both came from the drillhole field measurement of roof breaking movement [1–3]. The key stratum refers to the strata that plays a decisive role on the rock mass in whole or in part when there are multiple layers of hard strata in the overburden of the stope. The former can be called the key stratum of strata movement, and the latter is critical stratum [1]. The breakage of the key stratum will cause the breakage of all or part of the overburden strata and causes a large range of strata movement. If the rock structure is satisfied with the "S-R" stability after the break, it will form "voussoir beam" structure and continue to be the main carrier. Based on the "voussoir beam" theory, the overhanging "slab" mechanical model is established, which lays a theoretical foundation for the prediction of roof weighting. Meanwhile, the relationship and the monitoring principle of "support-surrounding rock" as well as the concept of green mining in coal mines are proposed [20, 21], which will made great contribution to ensure the safety of mining work.

The "voussoir beam" theory and key stratum theory also have great guiding significance in the field of shallow coal seam. Based on the key strata, load ratio, and burial depth as indicators, the definition of shallow coal seam is given [4], and the structure model of "step voussoir beam" of main roof is put forward [22–24]. According to field measurement and theoretical analysis, shallow coal seams can be divided into two types: (1) Typical shallow coal seams are characterized by shallow burial, small base load ratio, and single key stratum (SKS) structure. (2) Nearly shallow coal seams manifest as large bedrock thickness and small loose load layer thickness, which generally show two groups of key stratum with slight step subsidence. Researchers have proposed different roof structures according to different mining conditions, which effectively solves the problems of mining practice in shallow coal seam, for example, concentrated coal pillars [25–27], surface subsidence [28, 29], and water protection mining [30–32]. To solve the large deformation problem of gob-side entry retained mining, a negative Poisson's ratio (NPR) anchor cable supporting solution was designed based on the principle of energy coupling support and field tests were carried out [33–36]. However, the roof structure is mainly based on theoretical models proposed by support load measurement, physical simulation, and numerical calculation. There is no systematic study of roof structure field measurement in shallow coal seam. The field measurement of the movement of the roof rock layer is mostly based on vertical drillhole observations on the ground surface of the working face; this method is mainly to observe the heights of the fractured zone and the caved zone, but the cost is expensive and the observation time is long [37–39]. The location and intensity of the broken zone of the working face can be more accurately grasped by using of the indirect observation method, but it is difficult to seize the true situation of the roof breakage and structural movement.

The Shenfu Dongsheng coal field in China is one of the largest coal fields in the world. The main coal seam in this area is a shallow seam of Jurassic age. The thickness of coal seam is 3.5~8 m, and the depth is less than 250 m [4, 12]. The 2^{-2} coal seams have wide occurrence in the Shenfu mining area, which are shallowly buried and have large recoverable thickness. Besides, the overburden bedrock is thin and the thickness of the loose layer is large, which is manifested as a single key stratum structure [30]. Shallow coal seam causes strong roof pressure and threat to the fragile environment during period weighting [2–4], as shown in Figure 1. At present, the roof structure of shallow buried working faces is mainly based on the theoretical models proposed by the measurement of support load, physical simulation, and numerical calculation [40–45]. With the continuous mining of 2-2 coal seam, the safety of stope and determination of working resistance in SBSKS have become a technical problem to be solved in the mining area. Therefore, in order to avoid the accidents in the roof caused by the large-scale weighting on the working face and ensure the safety during mining on the working face, the roof structure and determination of working resistance of SBSKS have important theoretical and practical guiding significance.

2. Grid Drillhole Field Method

2.1. Method Design. In order to reveal the roof structure shape during the mining process under the condition of SBSKS, the authors use multiple drillhole displacements and drilling peek in conjunction with the field measurement of the support load on the working face, which provides a scientific basis for the roof control of SBSKS mining. The authors have invented a field measurement method of grid drillhole. This method is suitable for three gateways arranged along the working faces. For example, there is 20~25 m section pillar between the auxiliary headgate gateway (AHG) and headgate gateway (HG). While ensuring the observation effect of the roof, the cost and construction volume of the drill site construction are considered, as shown in Figure 2.

The method includes setting multiple fixed stations in the AHG. The drillholes in the TA are divided into displacement inclined drillhole (DID) A_n, displacement vertical drillhole (DVD) B_n, and peek incline drillhole (POD) C_n; B_n and A_n are located on the same plane, and they intersect into mesh, while C_n is arranged parallel to the largest displacement incline drillhole. According to the drillhole and the inclination of the working face, the drillholes are divided into vertical drillholes and inclined drillholes in the tailgate airway (TA), as shown in Figure 3. Advanced drillholes in the TA are important sources to obtain advance fracture or movement information of the roof, which can accurately realize to early warning and forecast in mining.

Drillholes in the AHG can achieve the real-time monitoring of the whole process from before mining to after mining on the working face and satisfy the existing observation requirements for caved zones and fractured zones of roof overburden. Setting many fixed stations of measuring the AHG, the drillhole of each fixed measuring station includes displacement drillholes D_n, E_n, and F_n and peep drillhole, which are arranged parallel to the displacement drillhole F_n, as shown in Figure 4, where $n = 1, 2, 3 \cdots i$.

(a) (b) (c)

Figure 1: Ecological environment damage caused by mining: (a) surface cracks, (b) landslide, and (c) dead trees.

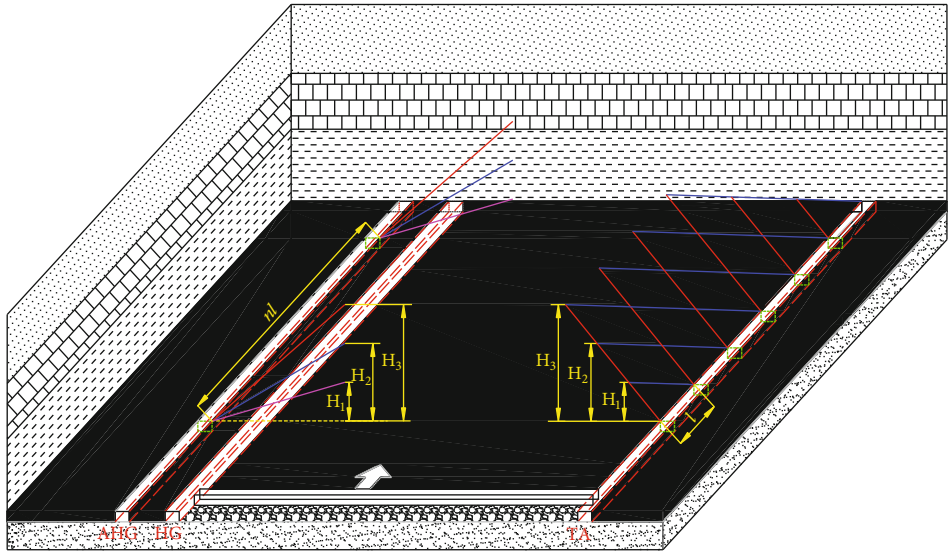

Figure 2: Schematic diagram of grid drillhole.

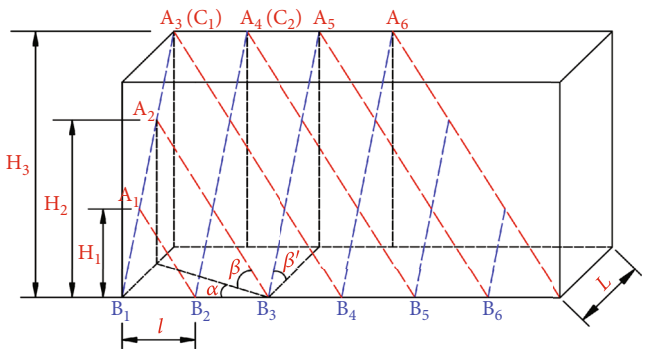

Figure 3: Schematic diagram of the drillhole space of the TA.

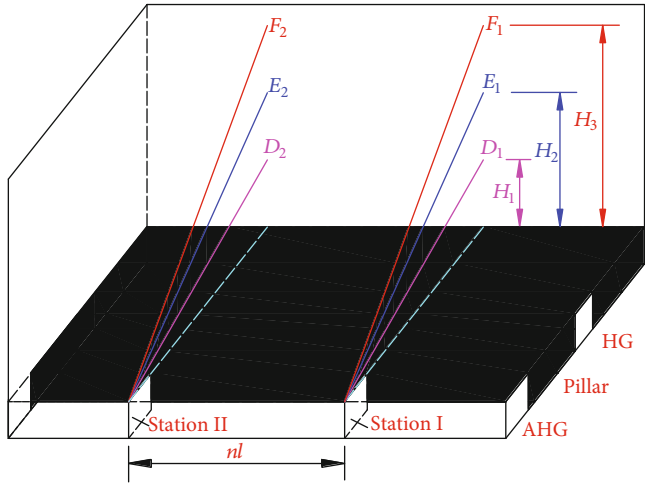

Figure 4: Schematic diagram of the drillhole space of the AHG.

2.2. Parameter Determination of Grid Drillhole Field Method. Due to the limitation of the underground mining and the working environment, we must consider the factors such as observation cost and quantity of observation works; the number of grid drillholes is not limited. The observation site and quantity are determined by the observation purpose.

Firstly, we must determine the level of the roof structure to be studied, that is, the vertical height of the drillhole. The maximum vertical height of the drillhole must exceed the

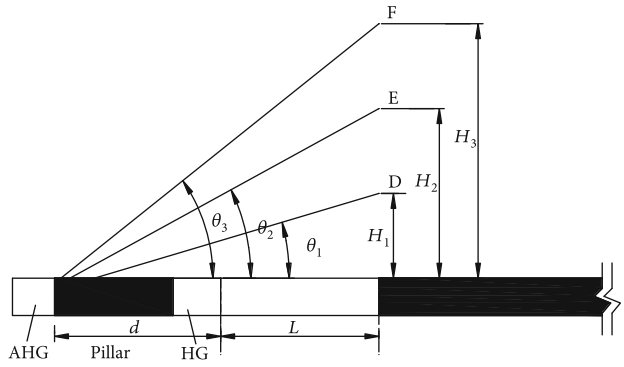

Figure 5: Sectional view of the drillhole of AHG.

main roof boundary of the key stratum, which can form the main roof structure, for example, $H_1, H_2, H_3 \cdots H_n$ in Figure 2. The determining principle is mainly considered from the following aspects: depth, mining height, thickness, and lithology of immediate roof and main roof. The observing horizon height of the roof structure is determined through combining with engineering practice analogy and theoretical analysis.

At present, according to research experience for stope in shallow coal seam [4, 42], the vertical height of the drillhole generally takes 4-6 times of the mining height. Among them, the equivalent immediate roof is 2~3 times, and the main roof is 3~6 times. The observation horizon can be divided into 2~3 horizons.

Secondly, the distance of the initial drillhole or station from the setup entry to the working face is L_0/m. According to the results of theoretical research, engineering practice, etc., the range of the first weighting intervals are obtained, so L_0 should be smaller than it. Meanwhile, we should select the same L_0 of the AHG and TA.

Thirdly, l/m is the horizontal distance of the adjacent drillholes in the TA, as shown in Figure 2. We refer to the results of engineering practice and theoretical research; l is smaller than l_z (l_z/m is the periodic weighting interval of the roof). For the fixed station of the AHG, the distance between two adjacent stations is nl, generally $n = 1 - 3$. The fixed measuring station must be arranged in the AHG, because it can meet the whole process of monitoring, while it cannot be observed when the working face is extracted in the TA. The drillholes of the fixed station include displacement drillholes and peek drillholes. The displacement drillholes need to be determined through the observation of the structure layer of the roof stratum. However, a vertical drillhole is usually arranged in the same position as the maximum displacement drillhole. The schematic of the drillholes of the fixed stations are shown in Figure 3.

The angle between the displacement drillholes D_n, E_n, and F_n of the fixed station in the AHG and the axial direction of the roadway is 90°, which is θ/° called elevation angle, as shown in Figure 5. The formula of θ is determined as

$$\theta_n = \arctan \frac{H_n}{L + \mathrm{d}} (n = 1, 2, 3 \cdots i), \tag{1}$$

where L/m is the horizontal distance of the overhang of the coal, L is the overhang distance in working face, m, and d/m is the width of the section pillar and the AHG.

According to the inclination of the drillhole and the working face, the designed drillholes in the TA are divided into vertical drillholes and inclined drillholes, and they are also divided into displacement vertical (inclined) drillholes and peek vertical (inclined) drillholes through their function. The vertical drillholes and inclined drillholes are in the same plane. The three-dimensional schematic of the drillhole are shown in Figure 3. The vertical drillholes and the inclined drillholes cross into a mesh. The angle between the inclined drillholes $(A_1, A_2, A_3 \cdots A_i)$ and the axial direction of the roadway is α/°; the elevation angle is β/°. The angle between the vertical drillholes $(B_1, B_2, B_3 \cdots B_i)$ and the axial direction of the roadway is 90°, while a/m is the horizontal distance between the DOD and the displacement incline drillhole. Combining the engineering practice with situation of construction safety, a is generally taken 0.5 m. Similarly, the elevation angle between the vertical drillhole and the horizontal plane can be calculated. The distance from the openings of the drillhole A, B, and C to the floor is determined by the specific section size of the roadway and the construction conditions of the drillhole.

The B_n, whose elevation angle is β_n/°, can be determined by the observation of the layer height H_n/m of the roof and the overhang distance L of the drillhole in the solid coal. Similarly, L generally takes great value, which is larger than the inclined length of overhang on the working face, and the elevation angle of the DVD is

$$\beta_n = \arctan \frac{H_n}{L} (n = 1, 2, 3 \cdots i). \tag{2}$$

The angle between the A_n and the axial direction of the roadway is α/°, which is determined through the distance l and L, as shown in Figure 3. The angle between the DID and the axial direction of the roadway is

$$\alpha = \arctan \frac{L}{\mathrm{nl}} (n = 1, 2, 3 \cdots i). \tag{3}$$

The elevation angle of A_n is β'/°, which is determined according to the H_n, l, and L, as shown in Figure 6. The elevation angle of the DID is

$$\beta' = \arctan \frac{H_n}{\sqrt{L^2 + (\mathrm{nl})^2}} (n = 1, 2, 3 \cdots i). \tag{4}$$

2.2.1. The Method for Determining the Broken Position of the Roof. The machine of YCJ90/360 drillhole peek was used to observe the broken position of internal drillhole, which can collect video, depth, inclination angle, etc. Besides, the post-processing software can calculate the vertical layer height of the broken roof and overhang distance (horizontal distance from the side of the pillar). According to comprehensive analysis, the broken structure of roof in strike and the

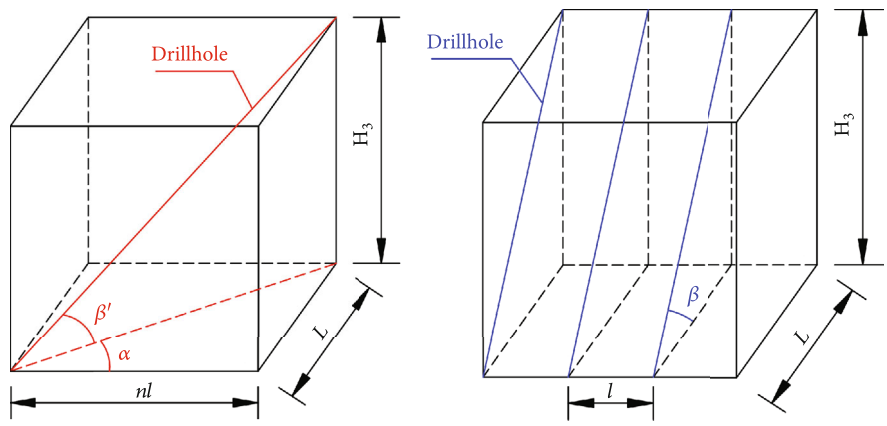

FIGURE 6: Sectional view of the drillhole of TA: (a) sectional view of A_n and (b) sectional view of B_n.

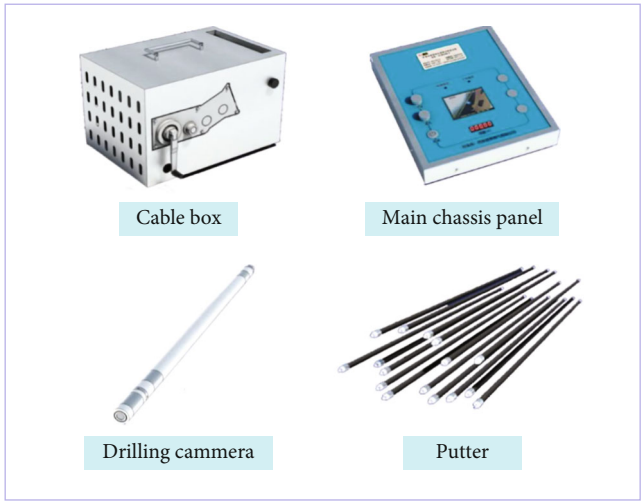

FIGURE 7: Equipment of drillhole observation.

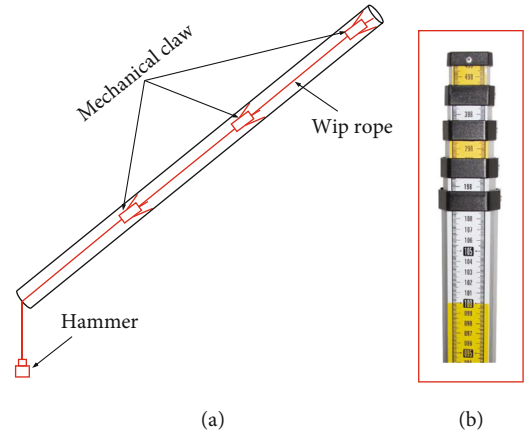

FIGURE 8: Equipment of the multipoint displacement meter and displacement measuring: (a) schematic diagram of a multipoint displacement meter and (b) 5 m measuring ruler.

broken structure of roof in inclination on the working face are obtained, as shown in Figure 7.

2.2.2. The Method of Roof Displacement Measurement. The meter of multipoint displacement is installed to observe the roof displacement. The displacement of the different roof layers is based on the initial value through the fixed point of floor corresponding to the displacement counterweight, and we used measuring rod for reading, as shown in Figure 8. A positive value indicates that the steel wire is pulled in, while a negative value indicates that the steel wire is spit out.

2.3. The Purposes of Grid Drillhole Field Method. Through installing displacement monitoring devices in each displacement drillhole in the drillhole field of the AHG and TA, the displacement change of roof in the drillhole can be monitored. The proposed method for the grid drillhole field in SBSKS is a coupling analysis method, which combines "field monitor of drillhole displacement, drillhole peek, and physical simulation." Compared with the current method and technology, this method can acquire a large amount of characteristic data from the roof movement and a wide observation range, which includes both the spatial position of the roof breakage and the displacement of the roof subsidence as well as the strength and the range of the damage. Therefore, it can fully reveal the structural characteristics of the roof movement in SBSKS, in order to realize the analysis of the roof structure shape and the movement process, including the height of the caving zone, the articulation layer of the roof, and the evolution of the broken angle.

During the process of mining on the working face, the drillhole peeker was employed to observe the drillhole continuously, so as to obtain the location of cracks, delamination, or cavings in the drillhole, and record the drillhole depth of each position (depth d_{ij}, where i is the number of the drillholes and j is the number of observations). Until the roof movement in the goaf of the working face is relatively stable, the final position of the break corresponding to each drillhole will be obtained.

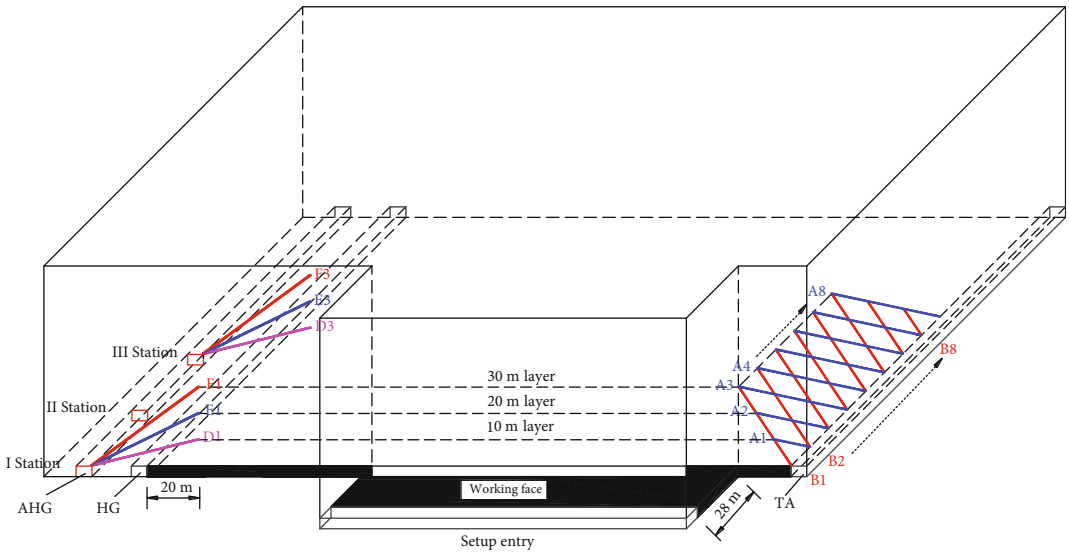

Figure 9: Schematic diagram of the filed construction of the grid drillhole in 22201 working face.

The horizontal distance l_{ij} from the orifice and the corresponding vertical height h_{ij} can be obtained by combining the drillhole angle α and the drillhole depth d_{ij} while solving different peek positions. By calculating all points of the broken position at each observation, the points in the drawing software were depicted to draw the evolution map of the broken position of the roof at different layers.

Drillholes can realize the real-time monitoring of the whole process of mining on the working face, revealing the relationship of the space and time between the movement and the weighting of the roof and verifying the size and the shape of the tip area on the working face that is inclined breakage. The advanced drillholes can monitor the overtime breakage or movement information of the roof and apply it to warn and forecast the weighting on the working face.

The quantitative calculation parameters of the roof structure were obtained, which provide important data to support the theoretical calculation. The conclusions include the determination of the broken expansion coefficient, the height of equivalent immediate roof.

By observing the breakage of the roof in each drillhole and collecting data to obtain the broken depth, then the vertical horizon height and lateral overhang distance of the broken roof are calculated, that is, the horizontal distance from the side of the coal pillar. Broken roof structure in working direction and in inclined direction according to comprehensive analysis.

2.4. Field Construction of Grid Drillhole. According to the above-mentioned design principles, 31 drillholes crossed into a mesh at the 22201 working face of Zhangjiamao Coal Mine in Shennan Mining Area of China. The average thickness of coal seam at 22201 working face is 8.0 m, the mining height was 6 m, the inclination angle was 1~2°, and the average buried depth was 76 m [41, 42]. The drillhole was continuously observed for about 60 days; meanwhile, the data of multipoint displacement meter and drillhole peek video for the first weighting and 5 times period weightings at 22201 working face were recorded totally. Based on the analysis of the measured data on field, the law of subsidence of the roof for the first weighting and the period weighting were obtained. The arrangement of drillhole in the AHG is shown in Figure 9. Among them Figure 6(a) expresses the section of inclination on the working face (AHG), while Figure 6(b) represents the section of strike on the working face (setup entry).

A total of 19 drillholes are arranged in the TA, which includes 11 inclined drillholes (including 3 peek drillholes) and 8 vertical drillholes, and the vertical drillholes and the inclined drillholes are on the same plane. The specific parameters are shown in Table 2.

3. Field Measurement and Analysis of Roof Structure of SBSKS

Observing the whole process of advance breakage, rotation, and continuously weighting of the roof and combining the field measurement of weighting on the working face revealed the structural form and movement law of the roof with large mining height in SBSKS. According to the roof displacement and its peek of the grid drillhole, the formation and the movement process of the roof structure were obtained during the first weighting and period weighting on the working face.

3.1. The Space-Time Relationship between the Movement and Weighting of the Roof. Through the field measurement of the drillhole and support pressure, during the first weighting, the roof movement obviously increased (up to 0.9 m) in the horizon of 8-10 m ahead of the working face, as shown in Figure 10(a). When the working face occurred the period weighting, the roof movement was ahead of the coal wall, as shown in Figures 10(b) and 10(c). In Figure 10, when the

Table 2: The information of drillhole layout at 22201 working face.

Position	Type	Vertical height (m)	Axial angle with roadway (°)	Elevation angle (°)	Length (m)	Quantity
AHG	DID	30	90	37	51.1	3
		20	90	27	45.7	3
		10	90	16	42.6	3
	PID	30	90	36	50.8	3
TA	DID	30	34	40	46.9	6
		20	34	40	31.3	1
		10	34	40	14.4	1
	PID	30	34	40	46.9	3
	DVD	30	90	56	36.1	6
		20	90	56	24.1	1
		10	90	56	12.1	1
Total					1291.2	31

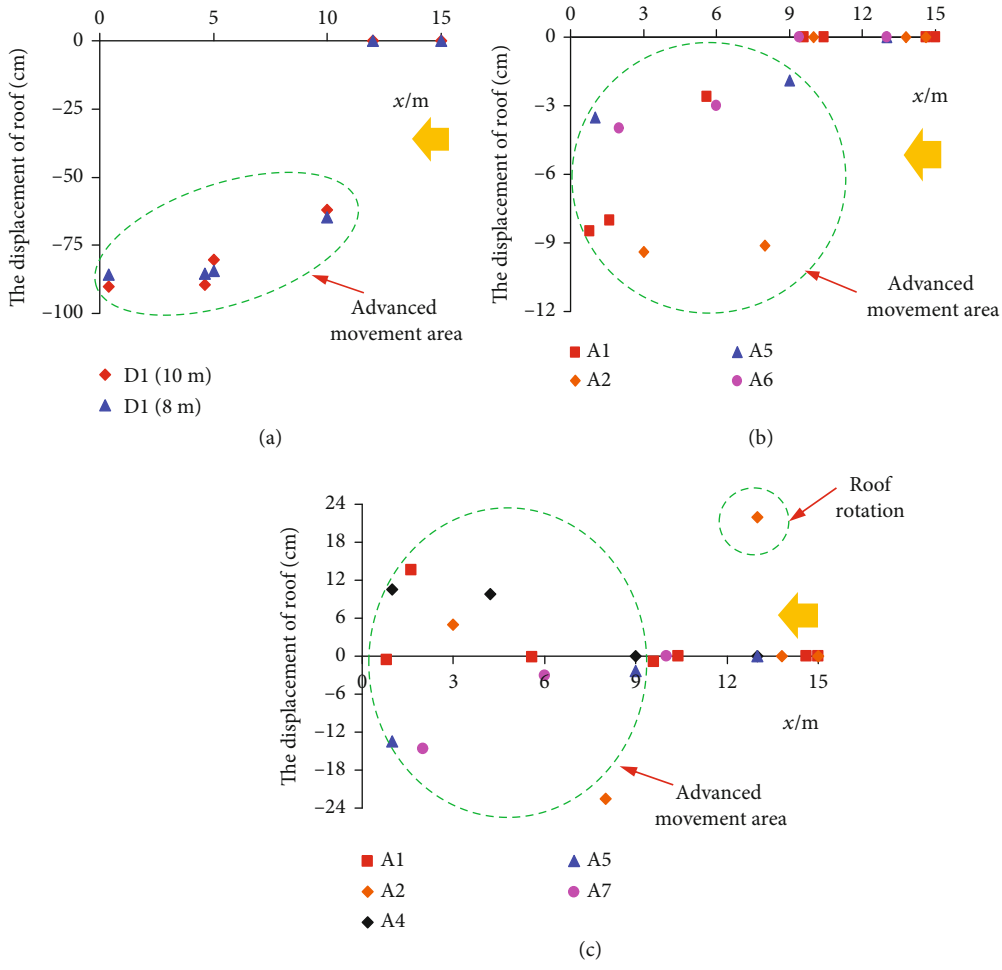

Figure 10: Overlying strata advanced breaking: (a) results of the D1 (10m) and D1 (8m); (b) results of the horizon of 10 m of A1, A2, A5, and A6; and (c) results of the horizon of 20 m of A1, A2, A4, A5, and A7.

working face is advanced to the observation station, the multi-point displacement meter can obtain the displacement of the different horizon of the roof. The results show that the field measurement result of the advanced breaking position of the 22201 working face is 5~10m, and the roof movement and the roof advanced breaking are ahead of the roof pressure.

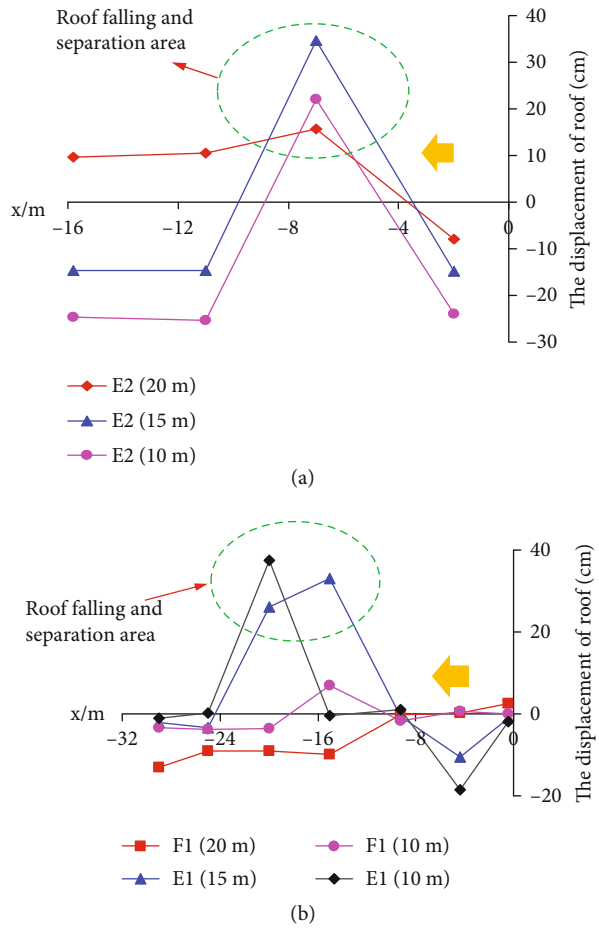

Figure 11: Overlying strata caved is lagging behind: (a) results of the I station and (b) results of the II station.

The 15~20 m horizon of the roof moved at the large range of 5~10 m behind the working face, and the roof falling and separation zone are mainly concentrated in the 15~20 m horizon of the roof, as shown in Figure 11. It indicates that the hinged layer is in 15~20 m horizon of the roof.

3.2. The Overburden Collapse Form on the Working Face and the Law of Roof Weighting. The experiment takes the 22201 large mining height working face of Zhangjiamao Coal Mine as the background. The simulation experiment has a geometric similarity ratio of 1 : 100. The model size is 200 cm (length) × 20 cm (width) × 84 cm (height). Select river sand as the aggregate, gypsum and white powder as the cementing material, and mica powder as the layered fissure material. According to the physical and mechanical parameters of coal and rock mass [41], according to similar conditions to determine the similar ratio of each rock layer, the experimental ratio table has a geometric similarity ratio of 1 : 100; see Table 3 for details.

When the working face advances to 31 m, the immediate roof caving, the caving height is 2.4 m. When the working face advances to 37 m, the immediate roof fully caving, the collapse height is 4.2 m, as shown in Figures 12(a) and 12(b).

When the working face advances to 48 m, the main roof first weighting, the caving height reaches 17 m, and the roof forms an asymmetrical three-hinged arch structure, as shown in Figure 12(c). When the working face is advanced to 60 m, the main roof first periodic weighting, the periodic weighting interval is 12 m, and the height of the roof caving zone reaches 17~19 m, as shown in Figure 12(d).

When the working face advances to 75 m, the main roof second periodic weighting, the periodic weighting interval 15 m, and the height of the roof caving zone is 28 m. The height of the roof caving zone which is originally 10~16 m is raised to 16~28 m, as shown in Figure 12(e). When the working face advances to 88 m, the main roof third periodic weighting, the periodic weighting interval is 13 m, the height of the roof fractured zone is 42 m, and the roof separation layer further develops upwards, as shown in Figure 12(f).

When the working face advances to 103 m, the main roof fourth periodic weighting, the periodic weighting interval is 15 m, the height of the roof fractured zone is 54 m, and the roof separation layer develops upward to the soil layer, as shown in Figure 12(g). When the working face advances to 119 m, the main roof fifth periodic weighting, the periodic weighting interval is 16 m, the roof fractured zone to the surface, the roof breaking angle behind the working face is 64°, and the loess roof breaking angle is 67°, as shown in Figure 12(h).

When the working face advances to 133 m, the main roof sixth periodic weighting, the periodic weighting interval is 14 m, and the overburden cracks develop to the surface, as shown in Figure 12(i). When the working face advances to 149 m, the main roof seventh periodic weighting, the periodic weighting interval is 16 m, and the surface form a sinking basin, as shown in Figure 12(j).

Through physical simulation, the first weighting interval of 22201 working face is 49 m, and the main roof breaks to form an asymmetrical three-hinged arch structure at the first time. The main roof forms a stepped rock beam hinged structure at the 18~26 m horizon, and the average periodic weighting interval is 14 m. Combined with the field measurement and analysis of the mining pressure law of the 22201 working face, the periodic weighting interval is 10~15.8 m, with an average of 13 m, indicating that the physical simulation experiment is basically consistent with the actual measurement results.

Based on the analysis of the floor's sensor, the distribution law of the front abutment pressure of working face is obtained, as shown in Figure 13. When the working face occurred in first weighting, the front abutment pressure peaks at 10~12 m before the work face, the maximum value is 2.90 MPa, and the peak factor is 1.61; during the period of periodic weighting, the front abutment pressure peaks at 8~15m ahead of the work face, and the peak coefficient is 1.74~1.86. The actual measured front abutment pressure peak is 8~10 m ahead the coal wall of the working face, and the peak coefficient is 1.7. The physical simulation results are consistent with the actual measurement results, indicating that the physical simulation is accurate and reliable.

Table 3: Material ratio of 22201 working face physical simulation experiment.

No.	Rock formation	Thickness of model (cm)	Thickness of each layer (cm) (time)	Material ratio	Consumables/kg			
					Sand	Gypsum	White powder	Fly ash/oil
12	Drift sand	12	2(6)	919	17.28	/	1.92	
11	Loess	17	2(8)	4.5 : 4.5 : 1	Sand: 8.64		Soil: 8.64	Oil: 1.92
10	Siltstone	21	3(7)	746	25.2	1.44	2.16	
9	Siltstone	3	3(1)	737	25.2	1.08	2.52	
8	Silty mudstone	3.5	3(1)	728	25.2	0.72	2.88	
7	Medium sandstone	2.5	3(1)	646	24.69	1.65	2.47	
6	Quartz mudstone	3	3(1)	646	24.69	1.65	2.47	
5	Coarse sandstone	6	2(3)	737	25.2	1.08	2.52	
4	Quartz mudstone	2	2(1)	646	16.46	1.10	1.65	
3	Muddy siltstone	1.5	2(1)	746	16.8	0.96	1.44	
2	Coarse sandstone	4	2(2)	646	16.46	1.10	1.65	
1	2^{-2} coal seam	8	4(2)	20 : 20 : 3 : 5	6.78	0.76	1.28	6.78

3.3. The Roof Structure during the Roof Weighting. The movement is stable after the working face is advanced to the fracture line, and the weighting is covered. The articulation layer of roof was gradually moved from 10~20 m to 16~30 m, as shown in Figure 14. According to the field results [41], similar results have been obtained through numerical simulation and physical similarity. It can explain the above phenomenon more intuitively, and make up for the shortcomings of discontinuous observation in the field.

The periodical weighting of the working face is divided into three stages: the front roof breaks before the weighting comes, the roof structure rotates when the weighting comes, and the roof structure slides after the weighting, as shown in Figure 15, providing a basis for building a roof structure model.

According to statistics on the locations where cracks, separation zone, or caving zone occur in the D, E, and F drillholes of the fixed station, the broken law in inclination of the roof on the working face would be obtained. The 10 m, 20 m, and 30 m layers of the roof collapsed layer by layer from the bottom to the top, forming an arched breaking shape at the end area, as shown in Figure 16(a). Based on the peeping results after the overburden are stabilized, as shown in Figure 16(b), the trigonometric function is used to convert the breaking angles of the three stations from 10~30 m to 65°, 66°, and 67.7°.

The results of comprehensive drilling peek showed that the height of the overburden caving zone was about 16 m, the articulated rock stratum is 16~30 m, and the roof occurred step subsidence, which could form the structure model of step voussoir beam. Meanwhile, the height of step sinking is about 1.7 m, the maximum width of the crack is 260 mm, and the distance between periodic cracks is 9~13 m, as shown in Figure 17.

3.4. Determination of the Roof Breaking Angle. According to the solution of elastic mechanics and rock mass mechanics, the force state of any unit body inside the rock beam of the key layer, on the plane where the angle of σ_x is α, the formula for the angle θ_1 between the maximum principal stress σ_1 and σ_x is

$$\theta_1 = 0.5 \arctan\left(2\tau_{xy}/\sigma_x - \sigma_y\right). \tag{5}$$

Based on references [44, 45], the stress decomposition amount of the rock beam of the key layer is derived, and it is introduced into Equation (5), and θ_1 is obtained:

$$\theta_1 = 0.5 \arctan\left(\frac{3L}{h}\right), \tag{6}$$

where L is the limit span of the rock beam of the key stratum, m, and h is the thickness of the rock beam of the key stratum, m.

In the mining of shallow coal seam, L is approximately equal to the period weighting interval of the working face, so L/h can be approximated as the lumpiness of the key block. According to the author's research results, the key block i of the step rock beam model is between 0.8~1.4 in shallow coal seam [4]. Equation (6) can be simplified as

$$\theta_1 = 0.5 \arctan 3i \,(0.8 < i < 1.4). \tag{7}$$

Therefore, the range of θ_1 is $33.7° < \theta_1 < 38.3°$.

According to the Moore Coulomb criterion, the strength effect of the structural plane in the strength characteristics of the rock mass is analyzed, and the shear fracture angle formed by the failure plane and the maximum principal stress plane ($\sigma_1 > \sigma_3$) is obtained when the rock fails in a certain direction. The angle β_0 with the maximum principal stress σ_1 is

$$\beta_0 = 45° — \varphi_0/2, \tag{8}$$

where φ_0 is the internal friction angle of the rock. The roof of the shallow coal seam in northern Shaanxi is a moderately stable roof, so the internal friction angle of the bedrock ranges from 28°~45°.

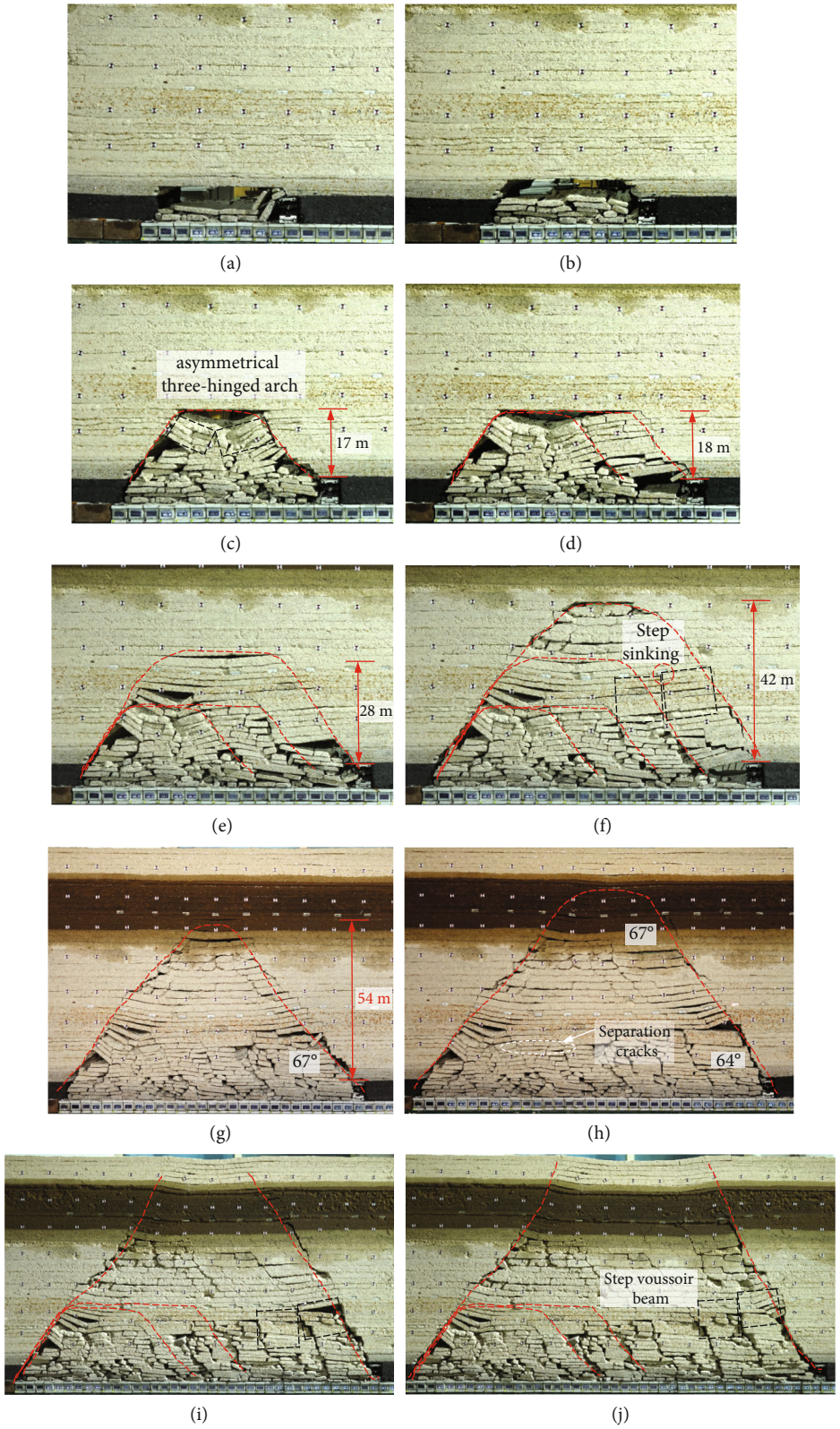

FIGURE 12: Physical simulation process of overburden cave law of the 22201 working face: (a) immediate roof caving, (b) immediate roof fully caving, (c) main roof first weighting, (d) main roof first periodic weighting, (e) main roof second periodic weighting, (f) main roof third periodic weighting, (g) main roof fourth periodic weighting, (h) main roof fifth periodic weighting, (i) main roof sixth periodic weighting, and (j) main roof seventh periodic weighting.

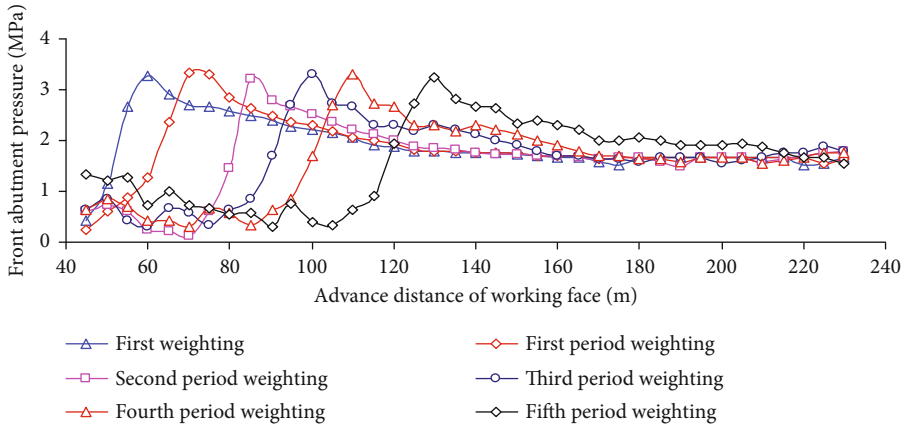

Figure 13: Distribution law of front abutment pressure in front of the working face.

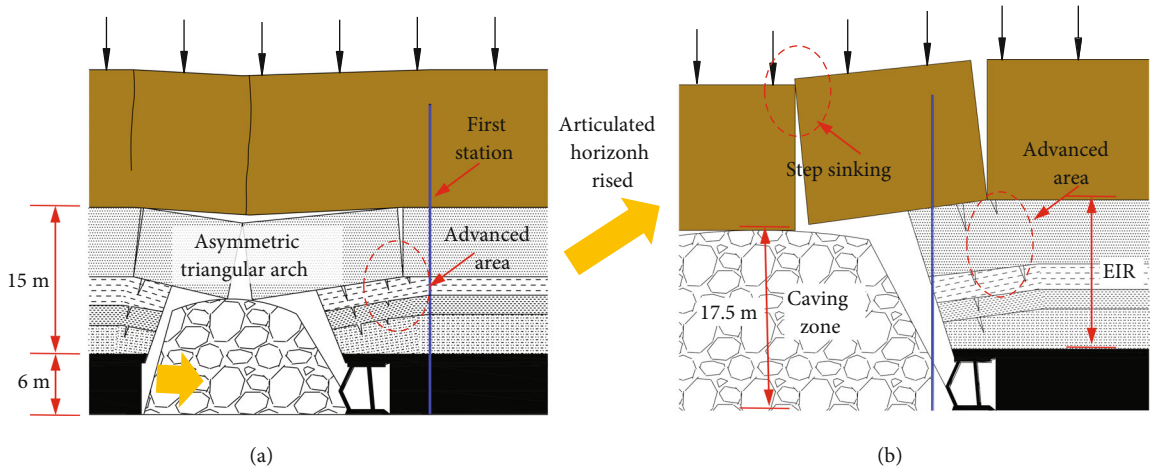

Figure 14: Schematic diagram of the evolution of the roof structure: (a) "asymmetric triangular arch" during the first weighting and (b) "stepped rock beam" during the period weighting.

In the above analysis, it can be concluded that the angle β between the fracture surface of the rock in the rock and the horizontal plane is

$$\beta_0 = 45^\circ - \frac{\varphi_0}{2} + 0.5 \arctan 3i. \quad (9)$$

Combining the values of various parameters, the roof breaking angle of shallow coal seam in Shenfu mining area ranges from 56.2° to 69.3°. Because there is a small internal friction angle of the soil layer, the breaking angle is larger than that of the bedrock.

Through the continuous peeping of the peep holes of the I station in AHG, when the working face advances to 66 m (the third periodic weighting was 63 m), it is ahead of the I station by 38 m, and the movement of the roof overburden tends to be stable; the peep results of D_1 and E_1 and peep holes of station I (as shown in Figure 18) can sketch the shape of the breaking angle of the roof.

According to the peek result in Figure 18, the corresponding horizontal distance can be calculated using mathematical knowledge. Therefore, based on the locations of the collapsed holes observed at different horizontal distances, it is calculated that when the mining height of the I station is 4.8 m, the bedrock breaking angle of the 10 m~20 m horizon is 71.5°, and the breaking angle of the 10 m~30 m horizon is 71.5°, and the average bedrock breaking angle is 65°.

In the same way, according to the analysis of the observation results in Figure 19. At the II station, when the mining height is 5.8 m, the bedrock breaking angle of the 10 m~30 m horizon is 74.4°~76.6°; at the III station, the bedrock breaking angle from 10 m~30 m levels is 67.7°.

By analyzing the influence of the thickness of the key stratum and the thickness of the load layer on the breaking angle, in the mining conditions of the 22201 working face, the thickness of the key stratum is in the range of 10 m~20 m, the roof breaking angle is 66°~68°, and the measured average breaking angle is about 68°, and the theoretically calculated breaking angle of the roof is 62.3°, which is basically consistent.

4. Determination of Working Resistance of Working Face of SBSKS

For the general filling type of large mining height in the working face, the key stratum of the main roof has a higher

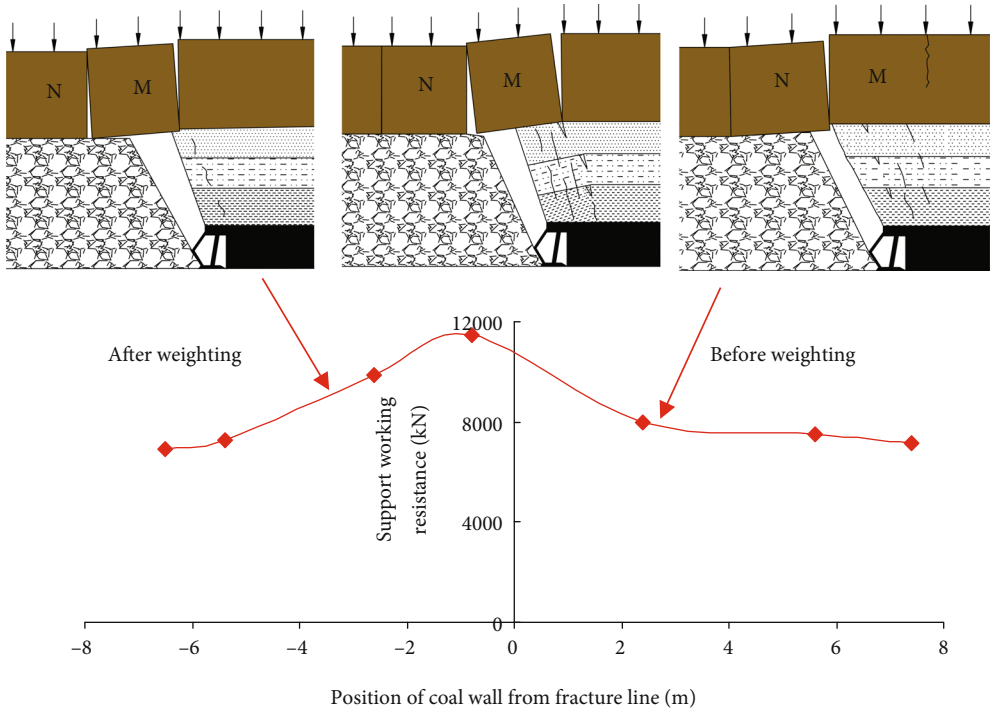

Figure 15: Three stages during the period weighting.

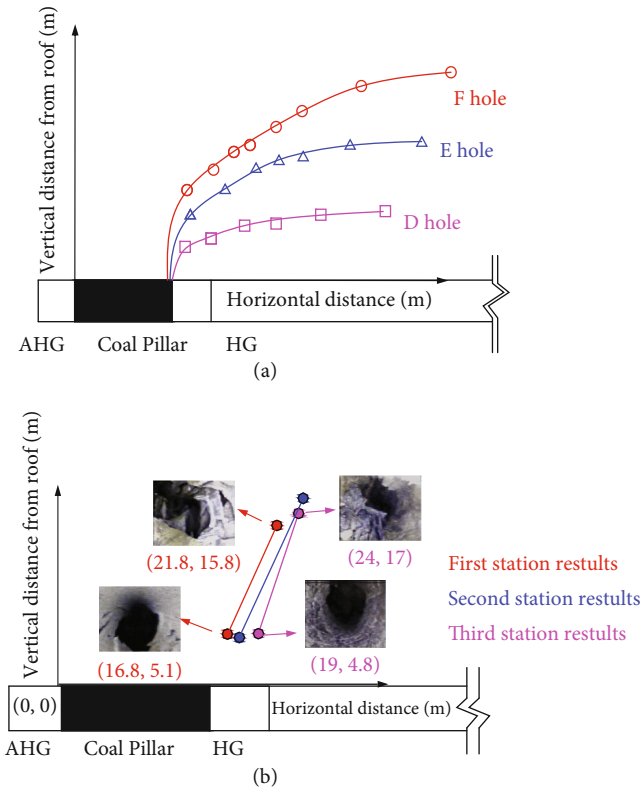

Figure 16: Schematic diagram of the evolution of roof structure: (a) inclined roof structure and (b) breaking angle.

hinge horizon and exists a step subsidence. Therefore, the "high position step voussoir beam" structure model of roof is established in high mining height working face in SBSKS. Figure 20 shows that m is the mining height, m; h_1 is the thickness of KS, m; $\sum h_i$ is the thickness of the EIR, m; h_2 is the thickness of EIR "short cantilever beam," m; h_3 is the thickness of easily caving EIR, m; M and N are the key blocks of "high position step voussoir beam" structure; R_1 is the force acting on the EIR from key block M, kN/f; R_2 is the weight of "short cantilever beam" EIR, kN/f; R_3 is the weight of easily caving EIR, kN/f; P_m is the support load, kN/f; A, B, and C are the hinge point of key blocks; d is the step height of rock blocks M and N, m; W is the amount of rotation subsidence of rock block N, m; and θ is the rotation angle of rock block M, °.

P_m can be calculated by using the following formula:

$$P_m = R_1 + R_2 + R_3, \tag{10}$$

where R_1 and R_2 and R_3 are calculated with support width B.

4.1. Stability Analysis of "High Position Step Voussoir Beam" Structure. According to the "step voussoir beam" theory [4], the mechanical model of "high position step voussoir beam" key blocks can be established as Figure 21. The key block N falls completely on the caving rocks, and the key block M is supported by the key block N at point C. At this point, the key block N is basically compacted, desirable $R_N \approx P_2$, $Q_B \approx 0$.

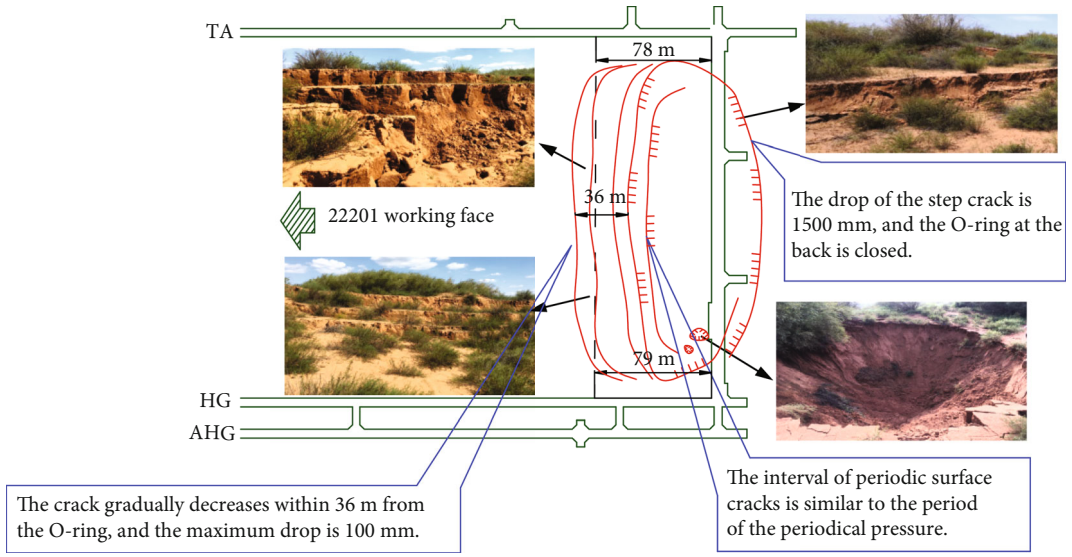

Figure 17: Schematic diagram of surface cracks during the mining.

(a) (b) (c)

Figure 18: When advancing to 66 m, peeping results of the I station: (a) the horizon of 5.1 m (suspension distance is 1.8 m) of D_1 hole collapsed, (b) the horizon of 9.3 m (suspension distance is 3.2 m) of E_1 hole collapsed, and (c) the horizon of 15.8 m (suspension distance is 6.8 m) of peep hole collapsed.

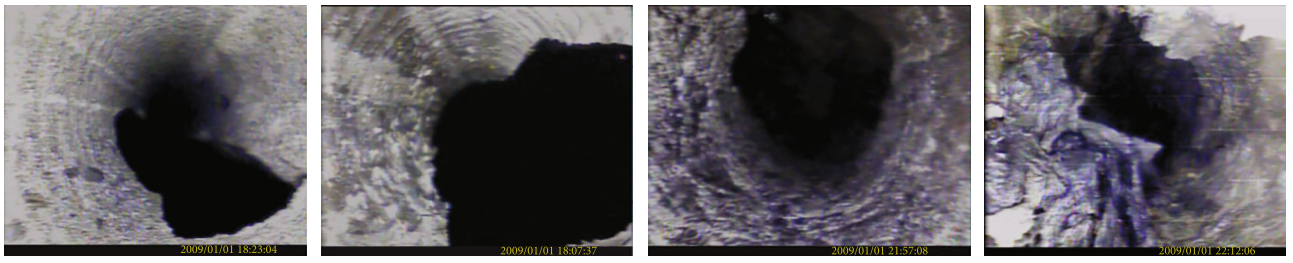

(a) (b) (c) (d)

Figure 19: Peeping results of stations II and III of the working face: (a) the horizon of 6 m (suspension distance is 6 m) of D_2 hole collapsed, (b) the horizon of 18.5 m (suspension distance is 9.5 m) of peep hole collapsed, (c) the horizon of 4.8 m (suspension distance is 2 m) of D_3 hole collapsed, and (d) the horizon of 17 m (suspension distance is 7 m) of peep hole collapsed.

The subsidence amount of the key block N is

$$W = m - (K_p - 1)\sum h_i = d + L\sin\theta. \quad (11)$$

Then,

$$d = m - (K_p - 1)\sum h_i - L\sin\theta, \quad (12)$$

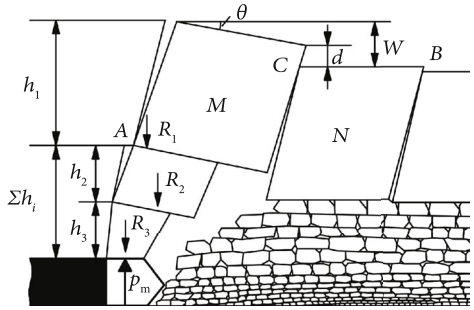

Figure 20: The mechanical model of "high position step voussoir beam" structure.

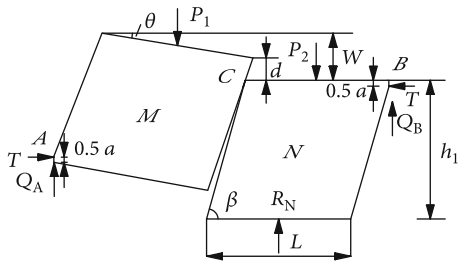

Figure 21: The mechanical model of "step" key blocks.

where W is the subsidence amount of the key block N, m; m is the mining height, m; K_p is the bulking coefficient of the rock mass in the gob after roof caving, set to 1.3; d is the step height of blocks M and N, m; and L is the length of the key block, m.

Take the torque for the key block M at point C, $\Sigma M_C = 0$:

$$T\left[\frac{h_1}{\sin\beta}\sin(\beta-\theta) - W - 0.5a\right] + P_1\left[\frac{L}{2}\cos\theta - d\cot(\beta-\theta)\right] - Q_A\left[L\cos\theta + \frac{h_1}{\sin\beta}\cos(\beta-\theta) - d\cot(\beta-\theta)\right] = 0, \tag{13}$$

where T is the horizontal squeezing force, kN; β is the breaking angle of the key stratum, °; h_1 is the thickness of key stratum, m; θ is the rotation angle of key block M, °; W is the subsidence height of key block N, m; a is the height of contact surface, m; P_1 is the sum of the weight of key block M and the overlying load, kN; L is the length of key blocks M and N, m; d is the step height of key blocks M and N, m; and Q_A is the shear force at point A, kN.

Taking the entire vertical force $\Sigma F_y = 0$, the equilibrium equation is as follows:

$$Q_A + Q_B + R_N - P_1 - P_2 = 0. \tag{14}$$

Substituting the $R_N \approx P_2$, $Q_B \approx 0$ through Equations (11)~(14), the T can be derived, as follows:

$$T = \frac{(h_1/\sin\beta)\cos(\beta-\theta) + (L/2)\cos\theta}{(h_1/\sin\beta)\sin(\beta-\theta) - W - 0.5a}P_1, \tag{15}$$

$$Q_A \approx P_1, \tag{16}$$

where Q_B is the shear force at point B, kN/m; R_N is the support force for key block N, kN/m; and P_2 is the sum of the weight of key block N and the overlying load, kN/m.

According to the "S-R" stability analysis, the "high position step voussoir beam" structure is easy to form sliding instability, and the condition for preventing the roof structure sliding instability is

$$T\tan\varphi + R_1 \geq Q_A, \tag{17}$$

where $\tan\varphi$ is the friction coefficient between the blocks, generally desirable 0.5, and R_1 is the support force for maintaining the stability of key block M, kN/f.

Through Equations (15)~(17), the supporting force for maintaining the stability of "high position step voussoir beam" structure is

$$R_1 = \left[1 - \frac{(h_1/\sin\beta)\cos(\beta-\theta) + (L/2)\cos\theta}{(h_1/\sin\beta)\sin(\beta-\theta) - W - 0.5a}\tan\right]P_1. \tag{18}$$

In Equation (18), the P_1 consists of the weight of key block M (R_G) and the weight of the load layer (R_Z):

$$P_1 = R_G + R_Z, \tag{19}$$

$$R_G = Bh_1L\gamma n \tag{20}$$

$$R_Z = K_G Bh_Z L\gamma_Z, \tag{21}$$

where B is the support width, m; γ is the bulk density of bedrock, kN/m^3; K_G (≤ 1) is the load transfer coefficient, h_z is the thickness of load layer, m; and γ_Z is the bulk density of load layer, kN/m^3.

Through Equations (18)~(21), the R_1 can be calculated by using the following formula:

$$R_1 = \left[1 - \frac{(h_1/\sin\beta)\cos(\beta-\theta) + (L/2)\cos\theta}{(h_1/\sin\beta)\sin(\beta-\theta) - W - 0.5a}\tan\right] \cdot (Bh_1L\gamma + K_G Bh_Z L\gamma_Z). \tag{22}$$

4.2. Determination of Rated Working Resistance at Working Face. The composition of support load of the " high position step voussoir beam " structure at longwall face is shown in Figure 22. The EIR cannot form a hinged structure, and its weight is all beared by the support.

$$R_2 \approx Blh_2\gamma, \tag{23}$$

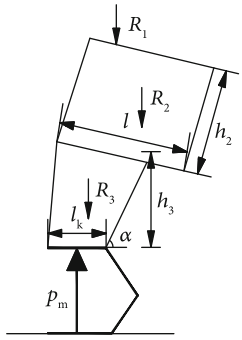

Figure 22: Load analysis model for support.

$$R_3 \approx B\left(l_k + \frac{1}{2}h_3 \cot \alpha\right)h_3\gamma, \tag{24}$$

where R_2 is the weight of "short cantilever beam" *EIR*, kN/f; R_3 is the weight of easily caving *EIR*, kN/f; B is the support width, m; γ is the bulk density of bedrock, kN/m^3; l is the length of "short cantilever beam," m; h_2 is the height of "short cantilever beam," m; l_k is the roof control distance of support, m; h_3 is the thickness of easily caving *EIR*, m; and α is the breaking angle of the EIR, °.

Through Equations (22) and (23) to Equation (24), the rated working resistance of support is

$$\begin{aligned} P_m = R_1 + R_2 + R_3 = B\left(lh_2 + l_k h_3 + \frac{1}{2}{h_3}^2 \cot \alpha\right)\gamma \\ + \left[1 - \frac{(h_1/\sin \beta)\cos(\beta - \theta) + L/2 \cos \theta}{(h_1/\sin \beta)\sin(\beta - \theta) - W - 0.5a} \tan \phi\right] \\ \cdot (Bh_1 L\gamma + K_G Bh_Z L\gamma_Z). \end{aligned} \tag{25}$$

Bringing Equation (11) into Equation (25), Equation (26) can be obtained:

$$\begin{aligned} P_m = B\left(lh_2 + l_k h_3 + \frac{1}{2}{h_3}^2 \cot \alpha\right)\gamma \\ + \left[1 - \frac{(h_1/\sin \beta)\cos(\beta - \theta) + (L/2)\cos \theta}{(h_1/\sin \beta)\sin(\beta - \theta) - m + (K_P - 1)\sum h_i - 0.5a} \tan \varphi\right] \\ \cdot (Bh_1 L\gamma + K_G Bh_Z L\gamma_Z). \end{aligned} \tag{26}$$

Considering the support efficiency, the working resistance of the support at working face is:

$$P = \frac{P_m}{\mu}, \tag{27}$$

where μ is the actual efficiency of support, set to 0.9.

As the mining height increases, the proportion of EIR load in the working resistance continues to increase. During the weighting, the EIR weight $R_2 + R_3$ accounts for 60%-65% of the rated working resistance, and the key stratum structure load R_1 accounts for 35%-40% of the rated working resistance. The weighting pressure load is caused by the movement of the key stratum structure, and it is caused by an increased pressure on the support. According to the structural mechanics model of the "high step rock beam" roof of large mining height face, the support resistance during nonpressure is the sum of the EIR weight $R_2 + R_3$ and the force during the noncompression of the key stratum.

4.3. Engineering Practice. According to the mining conditions of the 22201 working face in Zhangjiamao Coal Mine, the parameters are as follows: $m = 6$ m, $h_1 = 13$ m, $\sum h_i = 16$ m, $h_2 = 12$ m, $h_3 = 4$ m, $L = 13$ m, $l = 7$ m, $l_k = 5.6$ m, $\beta = 64°$, $\alpha = 64°$, $\theta = 8°$, $B = 1.75$ m, $\gamma = 24$kN/m^3, $K_G = 0.5$, $a = 0.5$, $\tan \varphi = 0.5$, and $Kp = 1.27$. The static load of the large mining height working face is composed of the caving EIR weight R_3 and the "short cantilever beam" weight R_2 formed by the EIR, which is brought into the calculation according to Equations (23) and (24). The static load can be obtained:

$$R_2 + R_3 = 4632.6kN. \tag{28}$$

According to the analysis, the height of the key block of the high position step voussoir beam is 13 m, and the load layer above the key stratum has weathered bedrock ($h_{ZF} = 13$ m) and loose sand soil layer ($h_{ZT} = 29$ m), whose bulk densities are $\gamma_{ZF} = 21$ kN/m^3 and $\gamma_{ZT} = 17$ kN/m^3.

The dynamic load of support of SBSKS structure R_1 is:

$$\begin{aligned} R_1 = \left[1 - \frac{h_1 \cot \beta + (L/2)}{2(h_1 - m + 0.27\sum h_i)}\right](Bh_1 L\gamma + K_G Bh_Z L\gamma_Z), \\ K_G Bh_Z L\gamma_Z = K_G BL(h_{ZF}\gamma_{ZF} + h_{ZT}\gamma_{ZT}). \end{aligned} \tag{29}$$

With the above parameters, the calculation is $R_1 =$ 6844.7kN/f.

Then the working resistance of support is $P = P_m/0.9 = (R_1 + R_2 + R_3)/0.9 = 12752.6$kN/f.

According to the field measurement, the average working resistance of the support is 10343 kN/f during the period weighting, the maximum working resistance of the support at the middle of the working face is 12049 kN during the weighting, and the opening rate of the safety valve is less than 8%. According to the established theoretical model of the roof structure, the maximum working resistance of the support is 12752.6 kN/f. The theoretical calculation is consistent with the actual and reliable basis. In summary, the utilization rate of support resistance is high, and the operation is safe and the support adaptability is better.

5. Results

(1) In this paper, the field measurement technology of grid drillhole is developed, and the roof breaking process and its movement track were detected, and then, the calculation formula of roof breaking angle was given. The broken law of the EIR was measured in practice, and then, the load and the bearing effects of the thick EIR were analyzed. Besides, the

phenomenon of "step subsidence " of the roof with large mining height working face was field proved. Meanwhile, the phenomenon of the upward movement for the hinged layer of the main roof and the movement process of the roof structure on the working face with large mining height in SBSKS was proved

(2) Based on the innovative methods and comprehensive analysis methods such as field measurement of drillholes, the form and the evolution process of the roof structure on the working face with large mining height in SBSKS were revealed. In terms of large mining height, the "asymmetry arch with three articulation structures" during the first weighting and the "high position step voussoir beam" during the period weighting were verified practically

(3) The space-time relationship was established between the movement of the roof structure and the weighting of the working face. The three-stage division of roof breaking movement and the behavior of the weighting are proposed, and then, the most dangerous state of roof was determined, which provided reliable basis for establishing roof structure model and determining reasonable support resistance

(4) According to the field measurement and theoretical analysis, the "high position step voussoir beam" structure model of large mining height in SBSKS is proposed, and the reasonable working resistance calculation equation for large mining height working face is given. During the field measurement, the maximum working resistance of the support during the period of weighting pressure is 12049 kN/f. The theoretical calculation of the maximum working resistance is 12752.6 kN/f, indicating that the theoretical model is reasonable and the calculation results are reliable

Data Availability

The data are available and explained in this article; readers can access the data supporting the conclusions of this study.

Conflicts of Interest

The authors declare no conflict of interest.

Authors' Contributions

Q.H. conceptualized the study; Q.H. and Y.H. designed the experiments; Q.H. and Y.H. validated the study; Y.H. was responsible for data curation; Q.H. supervised the study; Y. H. wrote the original draft; Q.H. and Y.H. wrote, reviewed, and edited the study; Q.H. supervised the study; Q.H. was responsible for project administration; Q.H was responsible for funding acquisition.

Acknowledgments

This research was funded by the National Natural Science Foundation of China, grant numbers 52074211 and 51674190, Natural Science Basic Research Program of Shaanxi, program no. 2019JLP-08, and 2019 Excellent Doctoral Dissertation Program of University, program no. PY19001.

References

[1] M. G. Qian, *A study of the behavior of overlying strata in long wall mining and its application to strata control; Strata Mechanics*, Elsevier Scientific Publishing Company, 1982.

[2] S. S. Peng and H. S. Chiange, *Longwall Mining*, Wiley, New York, 1984.

[3] M. G. Qian and H. C. Li, "The movement of overlying strata in longwall mining and it's effect on ground pressure," *Journl of China Coal Society*, vol. 2, pp. 1–12, 1982.

[4] Q. X. Huang, *Study on roof structure and ground control in shallow seam longwall mining*, China University of Mining and Technology press, Xuzhou, China, 2000.

[5] S. Gu, C. Wang, B. Jiang, Y. Tan, and N. Li, "Field test of rock burst danger based on drilling pulverized coal parameters," *Disaster Advances*, vol. 5, pp. 237–240, 2012.

[6] V. Frid and K. Vozoff, "Electromagnetic radiation induced by mining rock failure," *International Journal of Coal Geology*, vol. 64, no. 1-2, pp. 57–65, 2005.

[7] B. T. Brady, "Laboratory investigation of tilt and seismicity anomalies in rock before failure," *Nature*, vol. 260, no. 5547, pp. 108–111, 1976.

[8] H. He, L. M. Dou, S. Y. Gong, J. He, Y. L. Zheng, and X. Zhang, "Microseismic and electromagnetic coupling method for coal bump risk assessment based on dynamic static energy principles," *Safety Science*, vol. 114, pp. 30–39, 2019.

[9] P. Konicek, K. Soucek, L. Stas, and R. Singh, "Long-hole destress blasting for rockburst control during deep underground coal mining," *International Journal of Rock Mechanics and Mining Sciences*, vol. 61, pp. 141–153, 2013.

[10] G. K. Ghosh and C. Sivakumar, "Application of underground microseismic monitoring for ground failure and secure longwall coal mining operation: a case study in an Indian mine," *Journal of Applied Geophysics*, vol. 150, pp. 21–39, 2018.

[11] Q. Yuan, J. Chai, D. D. Zhang, J. X. Liu, Y. Li, and G. Z. Yin, "Monitoring and characterization of mining-induced overburden deformation in physical modeling with distributed optical fiber sensing technology," *Journal of Lightwave Technology*, vol. 4, pp. 881–888, 2020.

[12] Q. X. Huang, Y. P. He, and J. Cao, "Experimental investigation on crack development characteristics in shallow coal seam mining in China," *Energies*, vol. 12, no. 7, p. 1302, 2019.

[13] C. Y. Liu, H. M. Li, H. Mitri, D. J. Jiang, H. G. Li, and J. F. Feng, "Voussoir beam model for lower strong roof strata movement in longwall mining-Case study," *Journal of Rock Mechanics and Geotechnical Engineering*, vol. 9, no. 6, pp. 1171–1176, 2017.

[14] Z. Fang, "Technology of geophysical exploration of coal in China," *Chinese Journal of Geophysics*, vol. S1, pp. 396–407, 1994.

[15] Y. Yu, J. B. Bai, X. Y. Wang, and L. Y. Zhang, "Control of the surrounding rock of a goaf-side entry driving heading mining face," *Sustainability*, vol. 12, no. 7, p. 2623, 2020.

[16] J. W. Li and C. Y. Liu, "Spatio-temporal distribution and gas conductivity of overburden fissures in the mining of shallow thick coal seams," *European Journal of Environmental and Civil Engineering*, vol. 8, pp. 1019–1033, 2019.

[17] S. Mahdi and C. L. Charlie, "Numerical modelling of longwall mining and stability analysis of the gates in a coal mine," *International Journal of Rock Mechanics and Mining Sciences*, vol. 51, pp. 24–34, 2012.

[18] S. R. Wang, X. G. Wu, Y. H. Zhao, P. Hagan, and C. Cao, "Evolution characteristics of composite pressure-arch in thin bedrock of overlying strata during shallow coal mining," *International Journal of Applied Mechanics*, vol. 11, no. 3, p. 1950030, 2019.

[19] J. W. Li, X. T. Li, C. Y. Liu, and X. Y. Wu, "Dynamic changes in surface damage induced by high-intensity mining of shallow, thick coal seams in gully areas," *Advances in Civil Engineering*, vol. 2020, Article ID 5151246, 16 pages, 2020.

[20] X. X. Miao and M. G. Qian, "Research on green mining of coal resources in China: current status and future prospects," *Journal of Mining & Safety Engineering*, vol. 1, pp. 1–14, 2009.

[21] M. G. Qian, "On sustainable coal mining in China," *Journal of China Coal Society*, vol. 35, no. 4, pp. 529–534, 2010.

[22] Q. X. Huang, M. G. Qian, and P. W. Shi, "Structural analysis of main roof stability during periodic weighting in long wall face," *Journal of China Coal Society*, vol. 24, pp. 581–585, 1999.

[23] Q. X. Huang, "Experimental research of overburden movement and subsurface water seeping in shallow seam mining," *Journal of University of Science and Technology*, vol. 14, no. 6, pp. 483–489, 2007.

[24] Q. X. Huang, J. L. Zhou, L. T. Ma, and P. F. Tang, "Double key stratum structure analysis of large mining height longwall face in nearly shallow coal seam," *Journal of China Coal Society*, vol. 42, pp. 2504–2510, 2017.

[25] S. Dawid and B. Jarosław, "Analysis of the influence of dynamic load on the work parameters of a powered roof support's hydraulic leg," *Sustainability*, vol. 11, no. 9, p. 2570, 2019.

[26] Z. B. Yu, S. Y. Zhu, Y. Z. Guan, and D. X. Hu, "Feasibility of modifying coal pillars to prevent sand flow under a thick loose layer of sediment and thin bedrock," *Mine Water and the Environment*, vol. 4, pp. 817–826, 2019.

[27] Z. Q. Zhang, J. L. Xu, H. L. Liu, and H. W. Li, "Influencing laws study of depth of gully on dynamic strata pressure of working face in shallow coal seams," *Journal of Mining and Safety Engineering*, vol. 30, pp. 501–505, 2013.

[28] A. I. Sofianos, "Analysis and design of underground hard rock voussoir beam roof," *International Journal of Rock Mechanics and Mining Sciences*, vol. 33, no. 2, pp. 153–166, 1996.

[29] K. B. Singh, P. Kumar, S. Kiran, N. C. Saxena, and B. Singh, "Subsidence behavior of Motur clays," *Journal of Mines, Metals and Fuels*, vol. 2, pp. 93–100, 1992.

[30] S. M. Wang, Q. X. Huang, L. M. Fan, and W. K. Wang, *The key technology of water conservation mining in fragile ecologically mining coal resources*, Science Press, Beijing, China, 2010.

[31] A. Li, Q. Ma, Y. Q. Lian, L. Ma, Q. Mu, and J. B. Chen, "Numerical simulation and experimental study on floor failure mechanism of typical working face in thick coal seam in Chenghe mining area of Weibei, China," *Environmental Earth Sciences*, vol. 5, p. 118, 2020.

[32] H. Li, B. Y. Zhang, J. J. Wu et al., "Surface water resource protection in a mining process under varying strata thickness—a case study of Buliangou coal mine, China," *Sustainability*, vol. 12, p. 4634, 2018.

[33] F. N. Wang, Z. B. Guo, X. B. Qiao et al., "Large deformation mechanism of thin-layered carbonaceous slate and energy coupling support technology of NPR anchor cable in Minxian Tunnel: a case study," *Tunnelling and Underground Space Technology*, vol. 117, article 104151, 2021.

[34] C. Li, Z. Wu, W. L. Zhang, Y. H. Sun, C. Zhu, and X. H. Zhang, "A case study on asymmetric deformation mechanism of the reserved roadway under mining influences and its control techniques," *Geomechanics and Engineering*, vol. 5, pp. 449–460, 2020.

[35] G. Li, Y. Hu, S. M. Tian, M. weibin, and H. L. Huang, "Analysis of deformation control mechanism of prestressed anchor on jointed soft rock in large cross-section tunnel," *Bulletin of Engineering Geology and the Environment*, vol. 80, no. 12, pp. 9089–9103, 2021.

[36] M. Z. Gao, J. Xie, Y. N. Gao et al., "Mechanical behavior of coal under different mining rates: a case study from laboratory experiments to field testing," *International Journal of Mining Science and Technology*, vol. 31, no. 5, pp. 825–841, 2021.

[37] T. G. Zhu, W. P. Li, Q. Q. Wang, Y. B. Hu, K. F. Fan, and J. F. Du, "Study on the height of the mining- induced water-conducting fracture zone under the Q(2l) loess cover of the Jurassic coal seam in northern Shaanxi, China," *Mine Water and the Environment*, vol. 1, pp. 57–67, 2020.

[38] G. Wang, C. Fan, H. Xu, X. L. Liu, and R. Wang, "Determination of long horizontal borehole height in roofs and its application to gas drainage," *Energies*, vol. 11, no. 10, p. 2647, 2018.

[39] G. Wang, M. M. Wu, R. Wang, H. Xu, and X. Song, "Height of the mining-induced fractured zone above a coal face," *Engineering Geology*, vol. 216, pp. 140–152, 2017.

[40] H. Maleki, "Coal pillar mechanics of violent failure in U.S. Mines," *International Journal of Mining Science and Technology*, vol. 27, pp. 387–392, 2017.

[41] Q. X. Huang and Y. P. He, "Research on overburden movement characteristics of large mining height working face in shallow buried thin bedrock," *Energies*, vol. 12, no. 21, p. 4208, 2019.

[42] Q. X. Huang, Y. P. He, and F. Li, "Research on the roof advanced breaking position and influences of large mining height working face in shallow coal seam," *Energies*, vol. 13, no. 7, p. 1685, 2020.

[43] Y. P. He, Q. X. Huang, B. Q. Wang, Y. P. Miao, and J. Li, "Field-measurement study on roof breaking angle of working face with large mining height in shallow coal seam," *Journal of Mining and Safety Engineering*, vol. 4, pp. 746–752, 2019.

[44] J. P. Zuo, Y. J. Sun, and M. G. Qian, "Movement mechanism and analogous hyperbola model of overlying strata with thick alluvium," *Journal of China Coal Society*, vol. 6, pp. 1372–1379, 2017.

[45] X. S. Li, K. Peng, J. Peng, and H. H. Xu, "Effect of cyclic wetting-drying treatment on strength and failure behavior of two quartz-rich sandstones under direct shear," *Rock Mechanics and Rock Engineering*, vol. 54, no. 11, pp. 5953–5960, 2021.